Bulletin of the JSME Vol.14, No.3, 2020
Journal of Advanced Mechanical Design, Systems, and Manufacturing

Design of a rotational-to-linear motion transformer using a double eccentric crank

Jun NANGO*, Yutaka YOSHIZAWA**, Hiroto ANBE* and Kouhei MURAKAMI***
*Mechanical Systems Engineering,
Graduate School of Science and Engineering, Yamagata University
4-3-16 Jounan, Yonezawa-shi, Yamagata 992-8510, Japan
E-mail: nango@yz.yamagata-u.ac.jp
**Z Mechanism Technology Institute Co., Ltd.
1-2-67 Fukuda-machi, Yonezawa-shi, Yamagata 992-0033, Japan
***Department of Mechanical Systems Engineering, Yamagata University
4-3-16 Jounan, Yonezawa-shi, Yamagata 992-8510, Japan

Received: 12 June 2019; Revised: 4 September 2019; Accepted: 10 December 2019

Abstract
Slider-crank mechanisms are used as a rotational-to-linear motion transformer in positive displacement pumps, because such mechanisms are effective for generating high discharge pressure. The stroke of slider-crank mechanism in a water pump is twice the crank length and the connecting rod must be sufficiently long to avoid problems caused by the side force, thereby, limiting the extent to which a positive displacement pump can be miniaturized. Small pumps with high discharge pressure are expected to be used as the power source of a hydraulic actuator. In this study, a mechanism wherein eccentric cams replace a crank and a connecting rod is proposed, and the operating principle and characteristics of this mechanism are investigated. The mechanism has a stroke that is four times the crank length, and it is designed with reference to an Oldham coupling mechanism. Replacing a crank with an eccentric cam is expected to reduce vibration by reducing fluctuations in the position of the center of gravity, but a concern is that using an eccentric cam will cause friction loss. An experimental device is manufactured to investigate the driving torque and the vibration characteristics.

Keywords : Planar mechanism, Slider-crank mechanism, Oldham coupling mechanism, Water pump

1. Introduction

A slider-crank mechanism is used for conversion between linear and rotational motions and is used under high-pressure conditions in applications such as engines, compressors, and water pumps as shown in Fig.1. However, a slider-crank mechanism creates linear piston motion, a side force, as shown in Fig. 2, perpendicular to the direction of motion occurs between the cylinder sides and the piston head, causing problems such as vibration and short life span. Therefore, several trials were done to understand the phenomenon of the frictional resistance caused by the side force (Aritomi, et al., 2012; Fei, et al., 2013; Nakashima, et al., 2012; Noda, et al., 2013). To try to solve the problem, the mechanism using multiple sliders instead of the connecting rod is proposed (Yoshizawa, et al., 2016).

To avoid such problems, the connecting rod must be sufficiently long. Figure 3 shows the relationship between the length of the connecting rod and the component of force pushing the internal wall (side force). As shown in Fig. 4, the stroke of a slider-crank mechanism is limited to twice the crank length. These problems regarding side force and stroke length make it difficult to miniaturize positive displacement pumps.

Small and low vibration pumps with high discharge pressure are expected to be used as power sources for hydraulic actuators, such as in precision medical equipment.

When the planar mechanism is driven at a high speed, the problem of vibration occurs. In order to suppress the vibration, the shaking force and shaking moment need to be balanced by adding a counterweight or another linkage

Paper No.19-00310
[DOI: 10.1299/jamdsm.2020jamdsm0040]

(Arakelian and Smith, 2005).

And, by using a cam mechanism, an unprecedented mechanism is proposed (Komatsubara, et al., 2015).

In the present study, a mechanism is proposed wherein eccentric cams replace a crank and a connecting rod, and the operation principle and characteristics of this mechanism are investigated. The mechanism has a stroke that is four times the crank length, and it is designed with reference to an Oldham coupling mechanism. Replacing a crank with an eccentric cam is expected to reduce vibration by reducing fluctuations in the position of the center of gravity, but a concern is that using an eccentric cam will cause friction loss. An experimental device is manufactured to investigate the driving torque and the vibration characteristics.

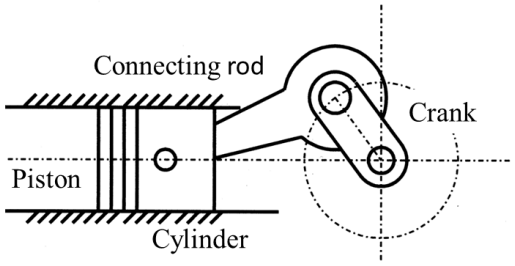

Fig. 1 Compressor as a typical application of a slider-crank mechanism. This mechanism allows high discharge pressure.

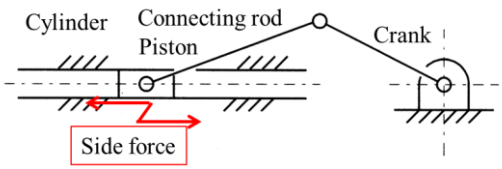

Fig. 2 Schematic of slider-crank mechanism. The crank and the connecting rod are each indicated by a representative straight line segment. White circles indicate revolute pairs. A side force acts on the piston as it moves in the cylinder, thereby causing contact with the internal wall.

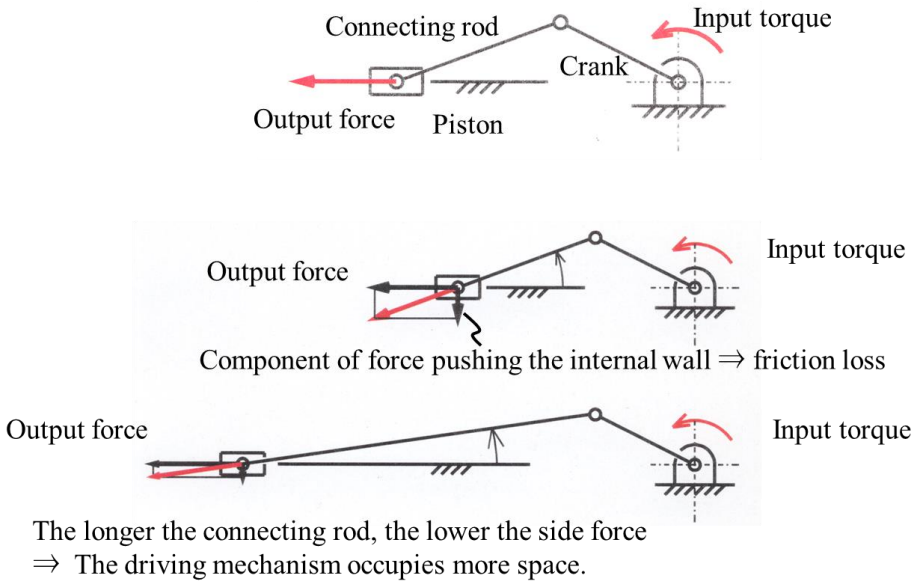

Fig. 3 The side force can be determined from the force of the component of the piston pushing against the internal wall. The longer the connecting rod, the lower the side force, but this comes at the expense of the driving mechanism requiring more space.

[DOI: 10.1299/jamdsm.2020jamdsm0040]

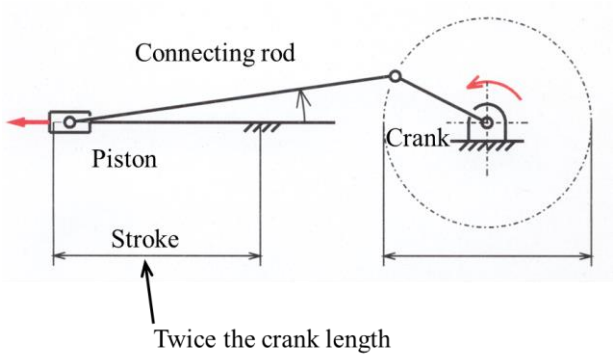

Fig. 4 Stroke of slider-crank mechanism. The stroke is twice the crank length.

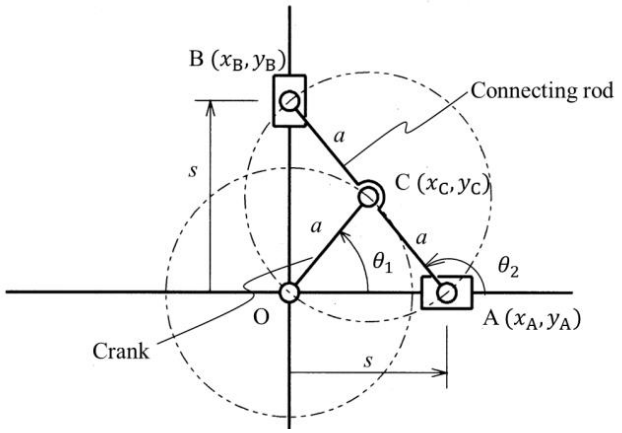

Fig. 5 Kinematic model of Oldham coupling mechanism. Representative pairs of points are indicated with A, B, C and O. Points A and B indicate revolute pairs, and prismatic pairs exist at the same points without the offset. The crank is linked with a revolute pair to the connecting rod to input the rotational motion.

2. Construction of mechanism

2.1 Oldham coupling mechanism

Figure 5 shows an Oldham coupling mechanism, where the rotational motion θ_1 is input about point O. When the crank of length a rotates counterclockwise, slider B is translated upward along the *y* axis and slider A is translated leftward along the *x* axis. The discharge pressure can be obtained by attaching a piston to slider A.

This mechanism has a stroke that is four times the crank length when the piston is attached on slider A, as shown in Fig. 6, because slider A can move both sides of crank shaft.

In this mechanism, to suppress fluctuation in the center of the mechanism and to make the components easy to integrate with an actuator, the crank and connecting rod are replaced with eccentric cams, as shown in Fig. 7.

[DOI: 10.1299/jamdsm.2020jamdsm0040]

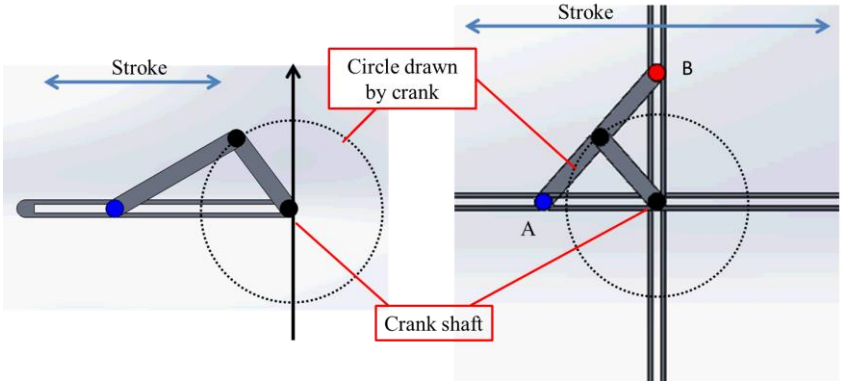

Fig. 6 Stroke comparison. The stroke of a slider–crank mechanism (left) is twice the crank length, whereas that of an Oldham coupling mechanism (right) is four times the crank length.

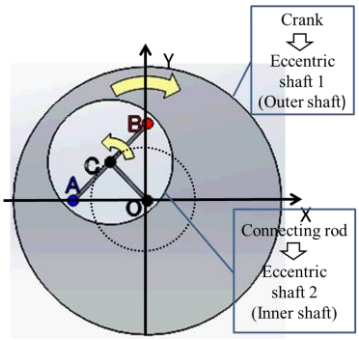

Fig. 7 Eccentric shaft. The crank is realized with eccentric shaft 1(outer shaft) and the connecting rod is realized with eccentric shaft 2 (inner shaft).

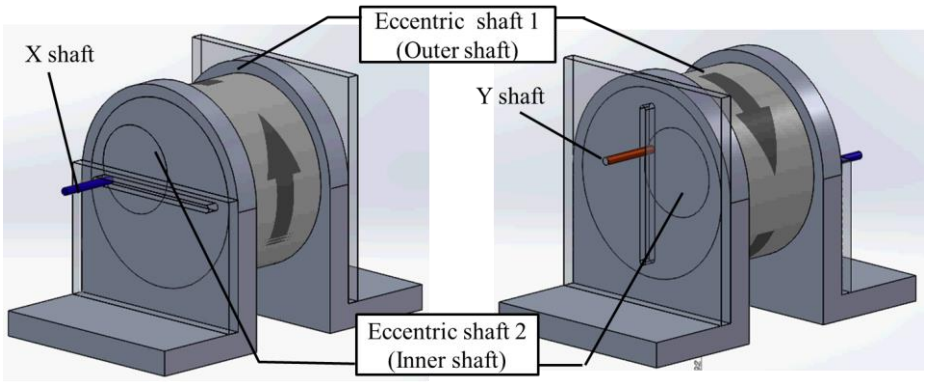

Fig. 8 Arrangement of orthogonal slider guides on either side of the mechanism. The X and Y shafts move horizontally and vertically, respectively, in their slits.

2.2 Rotational-to-linear motion transformer using a double eccentric crank

The construction of the mechanism proposed in this paper is shown in Figs. 7 and 8. The double eccentric crank comprises two eccentric cams. Two sliders, whose translational axes are perpendicular to each other, are arranged on the sides of eccentric shaft 1.

[DOI: 10.1299/jamdsm.2020jamdsm0040]

3. Dynamics analysis

Dynamics analysis was performed to verify the measurement values needed to drive the water pump. Figure 9 shows the free-body diagram of the mechanism using the double eccentric crank. In the kinematic diagram shown in Fig. 5, the crank is used to input the driving torque, but in the free-body diagram shown in Fig. 9, the crank is not used because the mechanism is over-constrained. To calculate the value of input torque for this mechanism, the input torque is given at the connecting rod.

Simultaneous linear equations are derived by balancing the forces and moments acting on each link when $\boldsymbol{F}_L$ is loading on the piston. By solving these simultaneous linear equations, the equation for calculating the input torque can be obtained, as shown in Eq. (1).

$$M_{Dz} = a\left\{-a\dot{\theta}_1{}^2(m_2 + 4m_3)\sin\theta_1 + (m_2 + 2m_3)g\right\}\cos\theta_2 + a\left\{-a\dot{\theta}_1{}^2(4m_1 + m_2)\cos\theta_1 - 2F_{Lx}\right\}\sin\theta_2 \quad (1)$$

Here,

$$\boldsymbol{M}_D = M_{Dz}\boldsymbol{k}, \quad F_{Lx} = |\boldsymbol{F}_L| \quad (2)$$

Where, m_1 , m_2 and m_3 indicate the mass of Link 1, Link 2 and Link 3, respectively.
Especially, when $m_1 = m_3$, the following equation is derived.

$$M_{Dz} = -a^2\dot{\theta}_1{}^2(4m_1 + m_2)\sin(\theta_1 + \theta_2) + a(m_2 + 2m_3)g\cos\theta_2 - 2aF_{Lx}\sin\theta_2$$

Because $\theta_1 + \theta_2 = \pi$, $\sin(\theta_1 + \theta_2) = 0$. So the following equation can be obtained.

$$M_{Dz} = a(m_2 + 2m_3)g\cos\theta_2 - 2aF_{Lx}\sin\theta_2 \quad (3)$$

While, the side force F_{14y}can be calculated from the following equation.

$$F_{14y} = a\dot{\theta}_1{}^2(m_2 + 2m_3)\sin\theta_1 - (m_1 + m_2 + m_3)g \quad (4)$$

$\boldsymbol{k}$ indicates the unit vector of the z-direction.

The free-body diagram of the slider-crank mechanism is shown in Fig. 10. Similar to the approach mentioned above, the input torque of the slider-crank mechanism can be calculated from Eq. (5).

$$M_{Dz} = \left(m_1\ddot{r}_{\mathrm{G}1y} + m_1 g\right)l_{G1}\cos\theta - m_1\ddot{r}_{\mathrm{G}1x}l_{G1}\sin\theta - (m_2\ddot{r}_{\mathrm{G}2x} + m_3\ddot{r}_{\mathrm{G}3x} - F_{Lx})a_1\sin\theta$$
$$+\frac{a_1\cos\theta}{a_2\cos\phi}\left[I_{2G}\ddot{\phi} - m_2\ddot{r}_{\mathrm{G}2x}l_{G2}\sin\phi - (m_3\ddot{r}_{\mathrm{G}3x} - F_{Lx})a_2\sin\phi + \left(m_2\ddot{r}_{\mathrm{G}2y} + m_2 g\right)\{a_2\cos\phi - l_{\mathrm{G}2}\cos\phi\}\right] \quad (5)$$

While, the side force F_{34y}can be calculated from the following equation.

$$F_{34y} = -m_2\ddot{r}_{\mathrm{G}2y} - (m_2 + m_3)g + \frac{1}{a_2\cos\phi}\left[I_{2\mathrm{G}}\ddot{\phi} - m_2\ddot{r}_{\mathrm{G}2x}l_{\mathrm{G}2}\sin\phi - (m_3\ddot{r}_{\mathrm{G}3x} - F_{Lx})a_2\sin\phi\right.$$
$$\left.+\left(m_2\ddot{r}_{\mathrm{G}2y} + m_2 g\right)\{a_2\cos\phi - l_{\mathrm{G}2}\cos\phi\}\right] \quad (6)$$

[DOI: 10.1299/jamdsm.2020jamdsm0040]

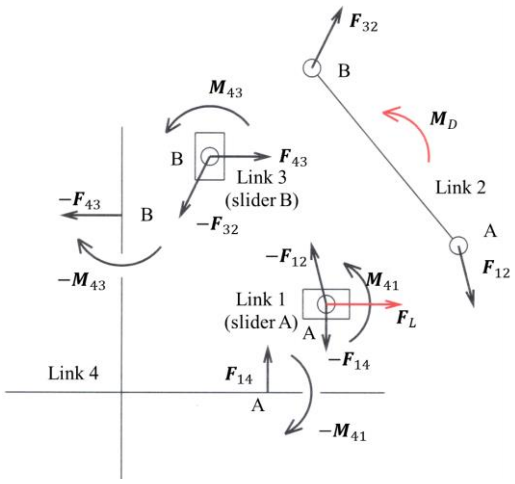

Fig. 9 Massless free-body diagram of the mechanism using a double eccentric crank. $\boldsymbol{F}_L$ and $\boldsymbol{M}_D$ indicate the load and the driving torque, respectively. $\boldsymbol{F}_L$ acts on the piston, which is transmitted through the piston rod, and finally acts on slider A. In this figure, the crank is removed from the mechanism, because this mechanism is over-constrained.

Here, a_1 indicates the crank length, a_2 indicates the connecting rod length, m_1 , m_2 and m_3 indicate the mass of Link 1, Link 2 and Link 3, respectively. l_{G1} and l_{G2} are parameters to locate the position of center of gravity of Link 1 and Link 2, respectively. $\ddot{r}_{\mathrm{G1}x}$, $\ddot{r}_{\mathrm{G2}x}$ and $\ddot{r}_{\mathrm{G3}x}$ indicate horizontal acceleration of center of gravity of Link 1, Link 2 and Link 3, respectively.

$\ddot{r}_{G1y}$ and $\ddot{r}_{G2y}$ indicate vertical acceleration of center of gravity of Link 1 and Link 2, respectively.

According to the result of the dynamic analysis, Eq. (3), the possibility of vibration suppression to be free of the influence of the rotational speed of the crank by the balancing of the weight of guide slider is shown. The fluctuation of the driving torque has a close relation with the cause of the vibration.

Namely, it indicates the possibility that the reduction of vibration is realized to be free of the influence of the rotational speed of the crank without a counterweight.

However, the result of the analysis is should be verified by experiments.

The results of the dynamic analysis are shown in Figs. 11 and 12. In this numerical calculation, values in the following are substituted.

$a = 0.010$, $a_1 = 0.020$, $a_2 = 0.060$, $l_{\mathrm{G1}} = 0.010$, $l_{\mathrm{G2}} = 0.030$ [mm] ,

$F_{Lx} = 25, 50, 100$ [N], $I_{2\mathrm{G}} = 1.986 \times 10^{-6}$ [kg · m^2]

In this graph, the rotational speed of the crank is 200[rpm], namely, $\ddot{\theta}_1 = \ddot{\theta} = 20.944$ [rad/s].

In these graphs, values of the input torque and the side force of the mechanism suggested in this paper are smaller than that of the slider-crank mechanism. In addition to the fluctuation of the driving torque, the value of the side force has a close relation with the cause of the vibration, too.

From Fig. 11, in any case, namely, the value of the magnitude of the load acting on the piston $F_{Lx} = 25, 50, 100$ [N], it can be confirmed that the amplitude of the input torque of the mechanism suggested in this paper is slightly smaller than that of the slider-crank mechanism.

From Fig. 12, regardless of the value of F_{Lx}, the side force is constant in the case of the mechanism suggested in this paper. That can be confirmed from Eq. (4). On the other hand, in the case of the slider-crank mechanism, the amplitude of the side force becomes larger as the value of F_{Lx} is larger.

Table 1 shows the mass of the main component of the driving mechanism.

[DOI: 10.1299/jamdsm.2020jamdsm0040]

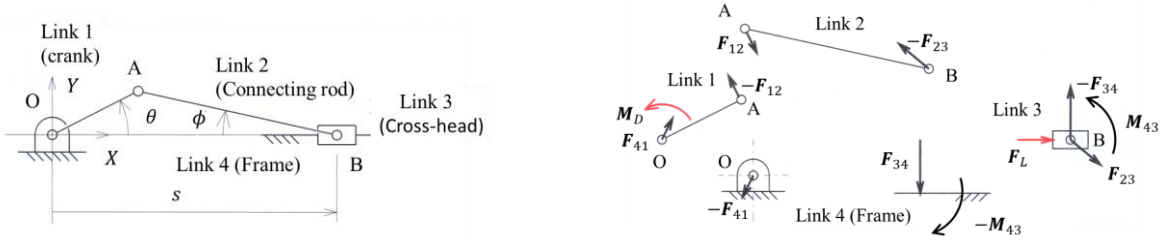

(a) Kinematic model of slider-crank mechanism (b) Massless free-body diagram of slider-crank mechanism

Fig.10 Kinematic model and mass-less free-body diagram of slider-crank mechanism. $\boldsymbol{F}_L$ and $\boldsymbol{M}_D$ indicates the load and the driving torque, respectively. $\boldsymbol{F}_L$ acts on the piston, which is transmitted through the piston rod, and finally acts on the cross-head. θ and ϕ indicate the crank angle and the swing angle of the connecting rod.

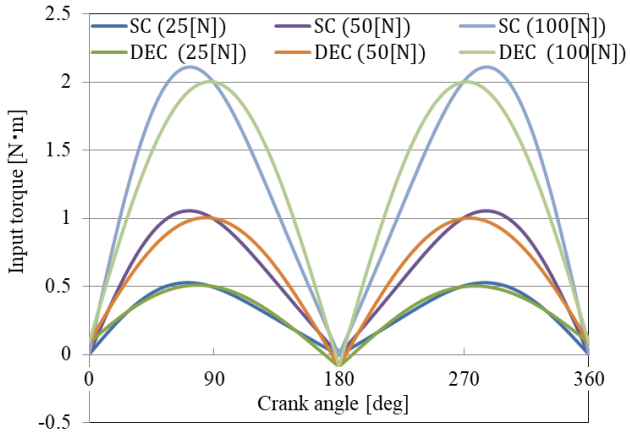

Fig.11 Input torque in dynamic analysis. SC and DEC stand for the slider-crank mechanism and the mechanism using a double eccentric crank, respectively. Figures in parentheses indicate the value of F_{Lx}. In any case, namely, the value of the magnitude of the load acting on the piston $F_{Lx} = 25, 50, 100$ [N], it can be confirmed that the amplitude of the input torque of the mechanism suggested in this paper is slightly smaller than that of the slider-crank mechanism.

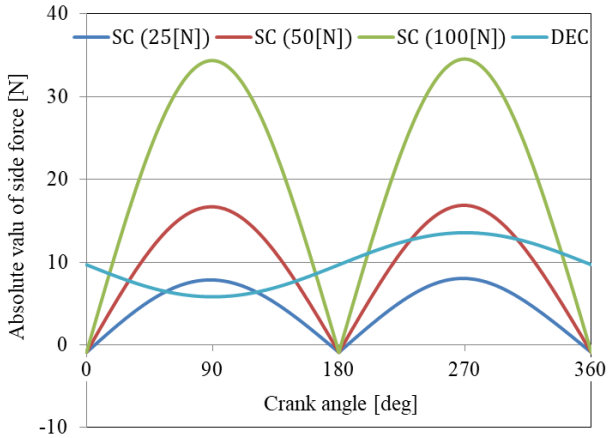

Fig.12 Side force in dynamic analysis. SC and DEC stand for the slider-crank mechanism and the mechanism using a double eccentric crank, respectively. Figures in parentheses indicate the value of F_{Lx}. Regardless of the value of F_{Lx}, the side force is constant in the case of the mechanism suggested in this paper. That can be confirmed from Eq. (4). On the other hand, in the case of the slider-crank mechanism, the amplitude of the side force becomes larger as the value of F_{Lx} is larger.

[DOI: 10.1299/jamdsm.2020jamdsm0040]

Table 1 Comparison of the mass of driving mechanism

	m_1 [kg]	m_2 [kg]	m_3 [kg]
Slider-crank mechanism	0.0261	0.0062	0.00862
Mechanism using double eccentric crank	0.1463	0.8013	0.0406

4. Design of experimental device

The experimental device is shown in Fig. 13. A motor is connected to the driving shaft of the crank through a torque transducer. The rotational driving motion is transmitted by a belt-and-pulley mechanism in which the pulley is attached the outside of eccentric shaft 1.

As shown in Fig. 14, the eccentricity is expanded by means of an additional crank, the use of which allows the diameter of the inner shaft to be reduced. The crank length is equal to the center distance so the diameter of the outer shaft can be reduced because a sufficient thickness can be obtained.

The composition of the experimental device is shown Fig. 15. The input torque is measured by a torque transducer. Under the same conditions, the input torque will be compared with that of a slider-crank mechanism.

Figures 16 and 17 show X shaft and Y shaft in the experimental device, respectively. In order to achieve smooth operation, and to reduce the sliding frictional resistance, the X shaft and Y shaft are attached to guide sliders. Teflon resin plates are put on the internal surface of the slit.

Figure 18 shows the top view of the driving mechanism. The driving rotational motion is transmitted by a belt-and-pulley mechanism. The piston rod is attached to the driving mechanism in parallel with the belt and X guide slider.

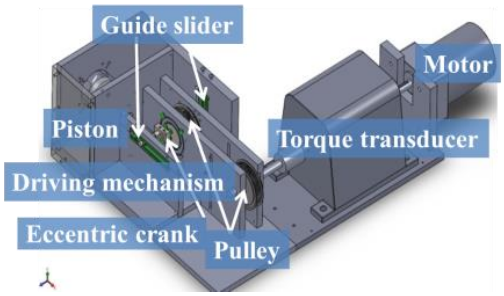

Fig. 13 Computer-aided drawing of experimental device composition. A motor is connected to the driving shaft of the crank through a torque transducer. The rotational driving motion is transmitted by a belt and pulley.

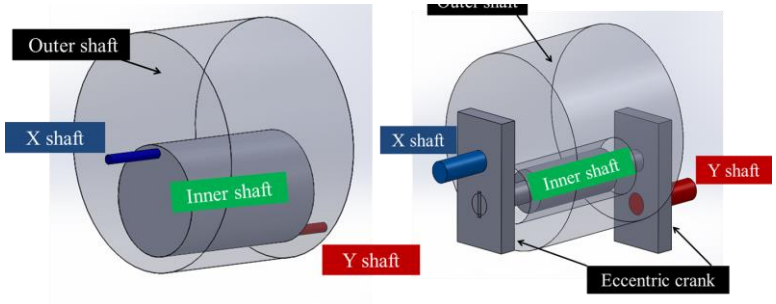

Fig. 14 Additional crank. Eccentricity is expanded by means of an additional crank, the use of which allows the diameters of the inner and outer shafts to be reduced.

[DOI: 10.1299/jamdsm.2020jamdsm0040]

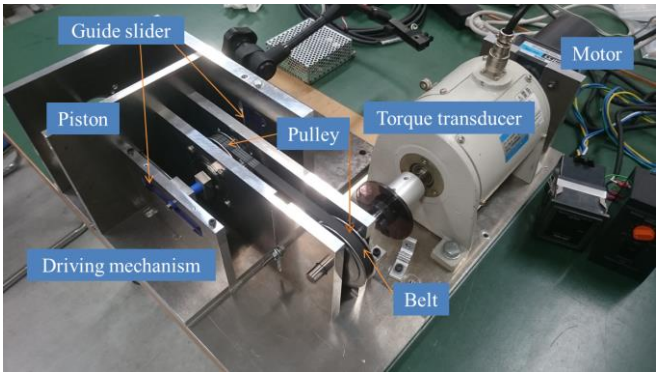

Fig. 15 Overview of the experimental system. The composition of the experimental device is shown in this picture.

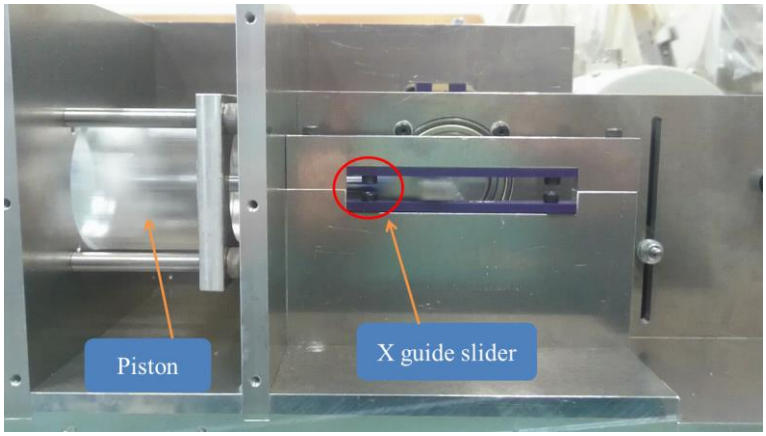

Fig. 16 Driving situation of the X slider. To achieve smooth operation, the X shaft is attached to a guide slider. To reduce the sliding frictional resistance, Teflon resin plates are put on the internal surface of the slit.

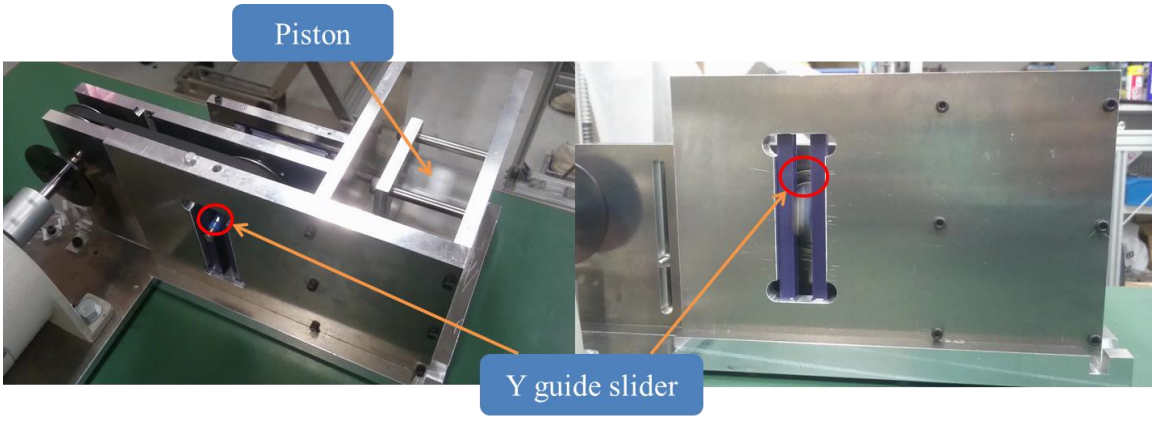

Fig. 17 Driving situation of the Y slider. As with the X slider, Y shaft is attached to a guide slider.

[DOI: 10.1299/jamdsm.2020jamdsm0040]

Figure 19 shows the experimental system to measure the input torque needed to drive the water pump using the mechanism with the double eccentric crank and the slider-crank mechanism. The input torque is measured when the water is circulated between the pump and the tank through pipes. Reed valves, shown in Fig. 20, is attached the wall on the cylinder head. The motor is connected to the crank shaft through a torque transducer (KYOWA TP-500GMCB).

Figure 21 shows the slider-crank mechanism to compare with the mechanism using the double eccentric crank. In this mechanism, a cross-head is attached to the piston to support the side force.

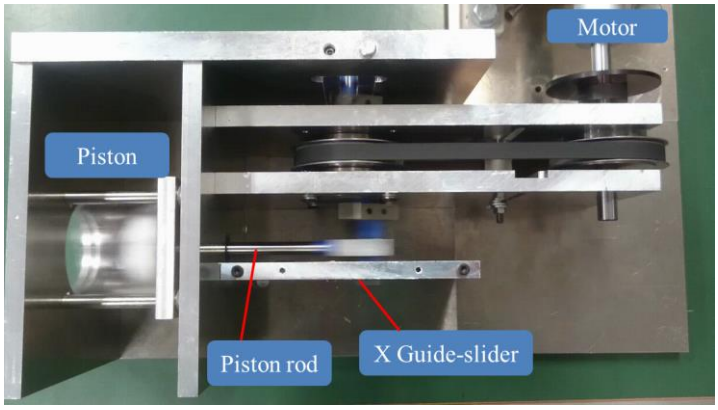

Fig. 18 Top view of the driving mechanism. The rotational driving motion is transmitted by a belt and pulley. The driving mechanism consists of the outer and inner shafts, which are arranged concentratedly in this part.

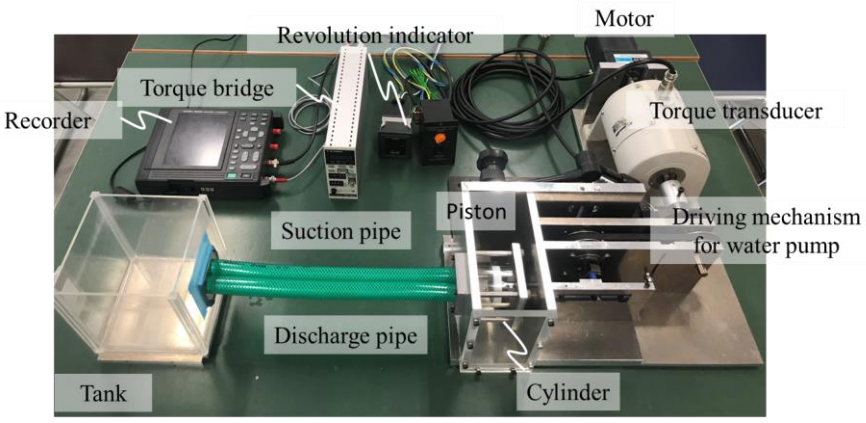

Fig. 19 Overview of the experimental system with the mechanism using a double eccentric crank. The motor is connected to the driving shaft of the crank through a torque transducer, thereby allowing measurement of the input torque driving the pump. Water is circulated between the pump and the tank through valves and pipes.

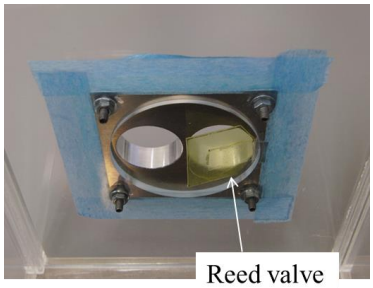

Fig. 20 Reed valve. The thin plates are opened and closed according to the pressure difference.

[DOI: 10.1299/jamdsm.2020jamdsm0040]

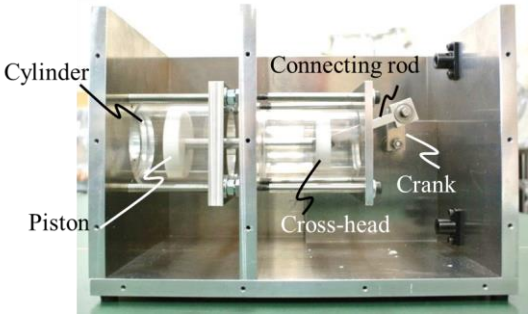

Fig. 21 Experimental water pump with slider-crank mechanism. In which, a cross-head is installed to support the side force. This is a similar mechanism to that used in diesel engines on large ships.

Table 2 Pump specifications

Experimental condition	
Diameter of piston	50 [mm]
Diameter of pipe	18 [mm]
Stroke	44 [mm]
Rotational speed	200 [rpm]

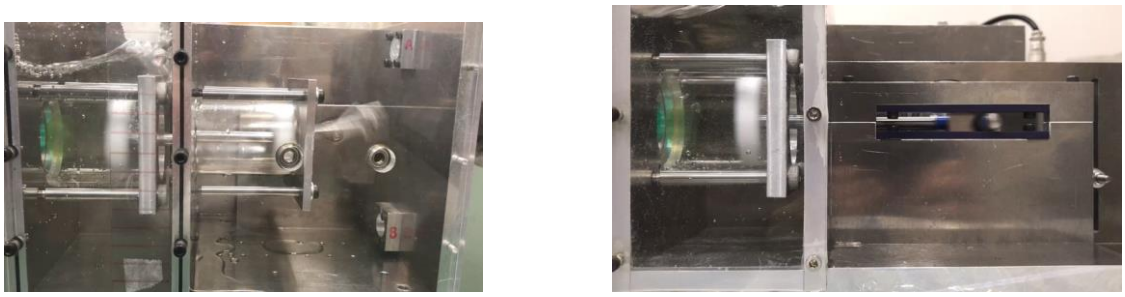

(a) Slider-crank mechanism with a cross-head (b) Mechanism using a double eccentric crank

Fig. 22 Experimental conditions. The crank rotates at 200 [rpm]. The cylinder is immersed in water.

Table 2 shows the pump specifications using the experimental device. Figure 22 shows the experimental conditions to drive the water pump. The crank rotates at 200 [rpm].

Figure 23 shows how the vibrational acceleration in the vertical direction is measured. The experiments are done under conditions in which one side of the cylinder is open to the air when the Teflon piston is moving in the acrylic pipe. At this time, the rotational speed of the crank is 200 [rpm].

The reason why the rotational speed of the crank is in a low speed area is that the influence of surface wave of water is reduced.

When the vertical vibrational acceleration is measured, the mechanism is used in a compressor, because the influence of surface wave should be reduced. And this low speed region is adopted to avoid the problem of heat production that causes at a cylinder (acrylic) and a piston (Teflon).

The materials of the frame of the experimental devices are made of aluminum alloy. A soft material such as rubber is put on the top board of the laboratory table. The frame made of aluminum alloy is supported on the table by rubber legs at multiple points.

If the problems of the surface wave of water in a water pump and the heat production that causes at a cylinder and a piston in a compressor can be solved, it is expected that the mechanism using a double eccentric crank can be driven in a high speed region.

[DOI: 10.1299/jamdsm.2020jamdsm0040]

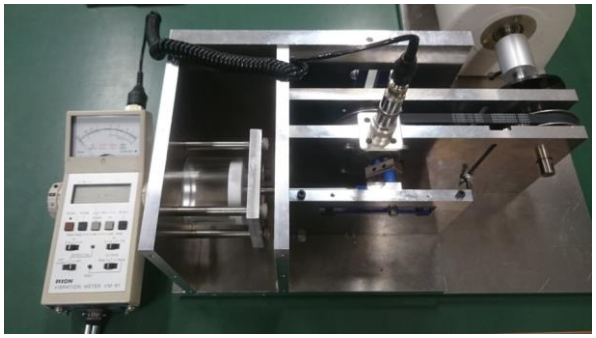

Fig. 23 Schematic of vibrational acceleration measurements. One side of cylinder is open to the air, a Teflon piston moves in the acrylic pipe, and the input rotational speed is 200 [rpm].

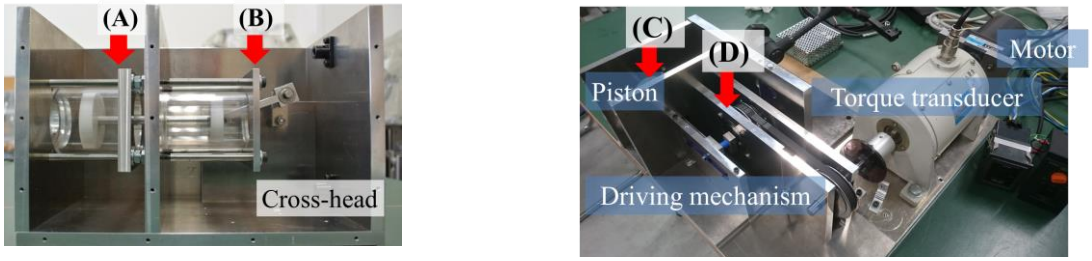

(a) Measurement points on a slider-crank mechanism with a cross-head

(b) Measurement points on mechanism using a double eccentric crank

Fig. 24 Measurement points for vibrational acceleration. Acceleration pickups are put on points (A) and (B) on the slider-crank mechanism. On the mechanism using double eccentric crank, acceleration pickups are put on points (C) and (D). In both of the case, the measuring points are on top of the driving mechanism and on the area around the cylinder.

Figure 24 shows the measurement points for vibrational acceleration. (A), (B), (C), and (D) indicate points where the acceleration pickups are placed. Measuring points are on top of the driving mechanism and on the area around the cylinder.

5. Experimental result

Figure 25 shows the results of measurements of input torque to drive the water pump. In this graph, the red line indicates the value in the case of the slider-crank mechanism. To compare the characteristics between these mechanisms, the blue line indicates the value in the case of the mechanism using double eccentric crank. The fluctuation and the maximum values in the case of the mechanism using double eccentric crank are smaller than that in the case of the slider-crank mechanism.

[DOI: 10.1299/jamdsm.2020jamdsm0040]

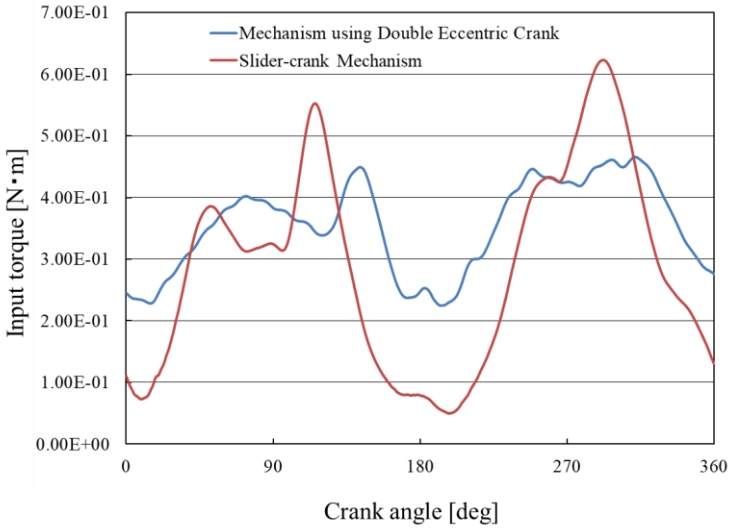

Fig. 25 Input torques of driving mechanisms of water pump. This graph shows the measured driving torque for each mechanism. The fluctuations and the maximum driving torque are smaller when using the double eccentric crank.

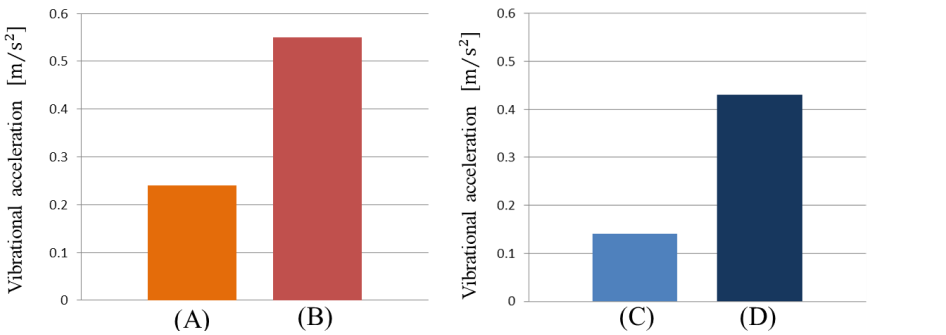

(a) Slider-crank mechanism (b) Mechanism using double eccentric crank

Fig. 26 Vertical vibrational acceleration of each mechanism. In both cases, on the top area around the driving mechanism, the vibrational acceleration is relatively large. It has to been considered that the experimental condition is not identical. Although there is a difference in mass, but the vibrational acceleration in vertical direction is smaller than that of slider-crank mechanism.

Figure 26 shows the results of the measurement of vertical vibrational acceleration of each mechanism. In both cases, on the top area around the driving mechanism, the vibrational acceleration is relatively large. The vibrational acceleration in the vertical direction is smaller than that of the slider-crank mechanism.

6. Conclusion

The mechanism proposed in this paper has been designed with reference to an Oldham coupling mechanism and comprises eccentric cams.

It was confirmed that the fluctuation and the maximum value of input torque of the mechanism suggested in this paper were smaller than that of the slider-crank mechanism when the water pump was driven by these mechanisms.

In the experiment measuring vertical vibrational acceleration, the value of the mechanism suggested in this paper was smaller than that of the slider-crank mechanism.

[DOI: 10.1299/jamdsm.2020jamdsm0040]

In the future, a method for evaluating vibrational suppression that considers the difference in mass must be investigated. In addition, it is our future work that the load acting on the guide slider is measured to realize to discharge high pressured air.

References

Arakelian, V., H. and Smith, M., R., Shaking force and shaking moment balancing of mechanisms: a historical review with new examples, Transactions of the ASME, Journal of Mechanical Design, Vol.127, MARCH (2005), pp.334–339.

Aritomi, S., Tokuo, K. and Miyazaki K., Quantification of contact force on sliding area of high-pressure fuel pump, Transactions of the Japan Society of Mechanical Engineers, Series C, Vol.78, No.793 (2012), pp.3178–3185 (in Japanese).

Fei, W., Fujita, N., Hirose, K. and Iwabuchi, A., Cylinder tribology in small two-stroke engine using the methanol fuel (comparison between engine test and sliding test), Transactions of the Japan Society of Mechanical Engineers, Series C, Vol.79, No.804 (2013), pp.2929–2938 (in Japanese).

Komatsubara, H., Kuribayashi, S., Hirata, K. andOhmachi, T., Development of new steam engine using the crown cam (1st Report, Design and production of prototype steam engine), Transactions of the JSME (in Japanese), Vol. 81, No. 825 (2015), DOI:10.1299/transjsme.15-00016.

Nakashima, K., Fuma, K., Kurokawa, D., Nakano, Y., Murakami, Y. and Yamamoto, M., Piston ring projection and catching in cylinder ports of two-stroke cycle engine, Journal of Advanced Mechanical Design, Systems, and Manufacturing, Vol. 6, No. 1 (2012),pp.23-32.

Noda, T., Shibata, E. and Ito, Y., Study on the friction characteristics of double reciprocating elements and micro surface textures, Transactions of the Japan Society of Mechanical Engineers, Series C, Vol.79, No.807 (2013), pp.4499–4512 (in Japanese).

Yoshizawa, T., Nango, J. and Koguchi, T., Experimental analysis of a water-pump driving mechanism using an orthogonal double-slider joint, Bulletin of the JSME mechanical engineering journal, Vol. 3, No. 1(2016), DOI:10.1299/mej.15-00551

[DOI: 10.1299/jamdsm.2020jamdsm0040]